Title
2-Arachidonoylglycerol Signaling in Forebrain Regulates Systemic Energy Metabolism

Journal
Cell Metabolism, 15(3)

ISSN
1550-4131

Authors
Jung, Kwang-Mook
Clapper, Jason R
Fu, Jin
et al.

Publication Date
2012-03-01

DOI
10.1016/j.cmet.2012.01.021

Published in final edited form as:
Cell Metab. 2012 March 7; 15(3): 299–310. doi:10.1016/j.cmet.2012.01.021.

2-arachidonoylglycerol signaling in forebrain regulates systemic energy metabolism

Kwang-Mook Jung[1], **Jason R. Clapper**[1], **Jin Fu**[1,3], **Giuseppe D'Agostino**[4,8], **Ana Guijarro**[1], **Dean Thongkham**[1], **Agnesa Avanesian**[1], **Giuseppe Astarita**[1,3], **Nicholas V. DiPatrizio**[1], **Andrea Frontini**[9], **Saverio Cinti**[9], **Sabrina Diano**[4,5,6,7], and **Daniele Piomelli**[1,2,3,*]

[1]Department of Pharmacology, University of California, Irvine, Irvine, CA 92697

[2]Department of Biological Chemistry, University of California, Irvine, Irvine, CA 92697

[3]Unit of Drug Discovery and Development, Italian Institute of Technology, Genova, Italy

[4]Departments of Obstetrics, Gynecology & Reproductive Sciences, Yale University School of Medicine, New Haven, CT 06520

[5]Neurobiology, Yale University School of Medicine, New Haven, CT 06520

[6]Section of Comparative Medicine, Yale University School of Medicine, New Haven, CT 06520

[7]Program on Integrative Cell Signaling and Neurobiology of Metabolism, Yale University School of Medicine, New Haven, CT 06520

[8]Department of Experimental Pharmacology, University of Naples "Federico II", Naples, 80131 Italy

[9]Department of Experimental and Clinical Medicine - Electron Microscopy Unit (Azienda Ospedali Riuniti), Università Politecnica delle Marche, 60020 Ancona, Italy

SUMMARY

The endocannabinoid system plays a critical role in the control of energy homeostasis, but the identity and localization of the endocannabinoid signal involved remain unknown. In the present study we developed transgenic mice that over-express in forebrain neurons the presynaptic hydrolase, monoacylglycerol lipase (MGL), which deactivates the endocannabinoid 2-arachidonoyl-*sn*-glycerol (2-AG). MGL-overexpressing mice show a 50 percent decrease in forebrain 2-AG levels, but no overt compensation in other endocannabinoid components. This biochemical abnormality is accompanied by a series of metabolic changes that include leanness, elevated energy cost of activity and hypersensitivity to β_3-adrenergic-stimulated thermogenesis, which is corrected by reinstating 2-AG activity at CB_1-cannabinoid receptors. Additionally, the mutant mice are resistant to diet-induced obesity and express high levels of thermogenic proteins, such as uncoupling protein-1, in their brown adipose tissue. The results suggest that 2-AG signaling through CB_1 regulates the activity of forebrain neural circuits involved in the control of energy dissipation.

*Corresponding Author: Dr. Daniele Piomelli, Department of Pharmacology, 3101 Gillespie NRF, University of California, Irvine, CA 92697-4625. Phone: (949) 824-6180 Fax: (949) 824-6305 piomelli@uci.edu.

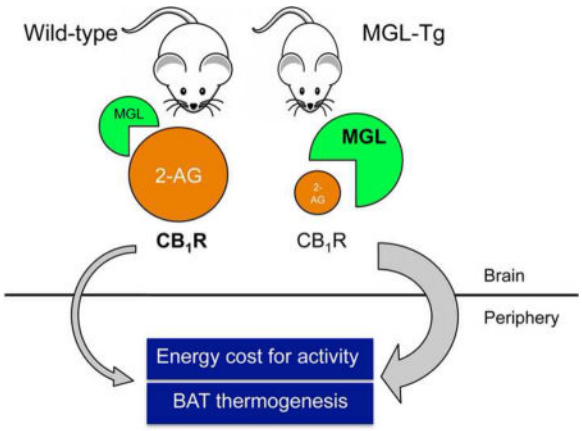

INTRODUCTION

Endocannabinoid signaling at CB_1 receptors plays a critical role in energy homeostasis (for review, see Mackie, 2006; Matias and Di Marzo, 2007). Preclinical and clinical studies have shown that CB_1 activation stimulates food intake (Kirkham, 2009), increases lipogenesis in white adipose tissue and liver (Cota et al., 2003; Osei-Hyiaman et al., 2005; Herling et al., 2008), and promotes insulin resistance in skeletal muscle (Eckardt et al., 2009). Conversely, pharmacological blockade or genetic ablation of CB_1 receptors decreases food intake, accelerates energy expenditure and corrects metabolic abnormalities associated with obesity in rodents (Matias and Di Marzo, 2007; Bajzer et al., 2011). Consistent with those data, clinical trials have shown that CB_1 inverse agonists are effective in lowering body weight and attenuating metabolic syndrome in obese human subjects (Ioannides-Demos et al., 2011).

While the studies outlined above underscore the importance of CB_1 receptors in metabolic control, they provide no information about the identity or localization of the endocannabinoid signals involved. Three lines of evidence point to a peripheral site of regulation (Kunos and Tam, 2011). First, feeding and obesity regulate the production of two endocannabinoid mediators – 2-arachidonoyl-*sn*-glycerol (2-AG) and anandamide – in peripheral tissues (Gomez et al., 2002; Engeli et al., 2005; Osei-Hyiaman et al., 2005). Second, CB_1 antagonists with restricted access to the brain retain the ability to reduce body weight gain and improve metabolic parameters in mouse models of obesity (LoVerme et al., 2009; Tam et al., 2010). Lastly, mutant mice that do not express CB_1 receptors in adipocytes display a lean phenotype (Mancini et al., 2010), while mice lacking CB_1 in hepatocytes are protected against diet-induced insulin resistance (Osei-Hyiaman et al., 2008).

Other evidence indicates, however, that endocannabinoid signaling in the central nervous system (CNS) also contributes to energy homeostasis (Matias and DiMarzo, 2007). In addition to modulating the hedonic properties of food, which can directly influence energy intake (Kirkham, 2009), CB_1 receptors in the brain may also control energy expenditure (Matias and Di Marzo, 2007). In the paraventricular nucleus of the hypothalamus, for example, CB_1 co-localizes with cocaine- and amphetamine-regulated transcript (CART) (Cota et al., 2003), a neuropeptide that regulates sympathetic activity and brown adipose tissue (BAT) thermogenesis (Elmquist, 2001; Abbott et al., 2001; Kong et al., 2003; Hentges et al., 2005; Tung et al., 2007; Smith et al., 2008). Confirming the functional significance of this localization, CB_1 deletion in mouse forebrain neurons causes a series of phenotypic changes that include leanness, resistance to diet-induced obesity and increased heat production (Quarta et al., 2010). A role for central endocannabinoid signaling in energy

homeostasis is further supported by the finding that leptin, an adipose-derived hormone that promotes energy utilization, inhibits endocannabinoid production in the rodent hypothalamus (Di Marzo et al., 2001), whereas the gastric hormone ghrelin, which promotes energy intake, exerts an opposite effect (Kola et al., 2008).

In the CNS, 2-AG is released by the action of two enzymes found in dendritic spine membranes: phospholipase C-β (PLC-β) and diacylglycerol lipase-α (DGL-α) (Stella et al., 1997; Hashimotodani et al., 2005; Tanimura et al., 2010). PLC-β hydrolyses phosphatidylinositol 4–5 bisphosphate to generate 1,2-diacylglycerol, which is cleaved by DGL-α to produce 2-AG (Stella et al., 1997). 2-AG travels across the synapse and inhibits neurotransmitter release by activating CB_1 receptors on axon terminals (Piomelli et al., 2007). This retrograde signaling process is interrupted by either of two intracellular 2-AG-degrading enzymes – monoacylglycerol lipase (MGL), which is localized to presynaptic terminals (Dinh et al., 2002; Gulyas et al., 2004), and α-β-hydrolase domain 6 (ABHD6), which is found in postsynaptic spines (Blankman et al., 2007; Marrs et al., 2010). As expected from the known functions of these enzymes, genetic deletion of DGL-α decreases, while deletion of MGL increases 2-AG content in the mouse brain (Tanimura et al., 2010; Gao et al., 2010; Chanda et al., 2010; Schlosburg et al., 2010). Ablation of DGL-α or MGL also causes, however, substantial changes in the steady-state levels of anandamide and arachidonic acid (Gao et al., 2010; Chanda et al., 2010; Schlosburg et al., 2010), which limits the usefulness of DGL-α- and MGL-null mice as models to define the central functions of 2-AG. In the present study, we generated transgenic mice that selectively over-express MGL in forebrain neurons. Compared to their wild-type littermates, these mutants show a 50 percent reduction in forebrain 2-AG levels, but no overt compensation in other components of the endocannabinoid system. Their metabolic phenotype suggests that 2-AG signaling through CB_1 regulates the activity of forebrain neural circuits that control energy expenditure.

RESULTS

Generation of MGL-Tg Mice

We created transgenic mouse lines that over-express MGL in the forebrain under the control of the CaMKIIα promoter (MGL-Tg mice; Figure 1A). The transgene-encoded MGL was fused with a V5 tag, which did not affect enzyme activity (Figure S1A). Founders were generated by pronuclear injection, and mutants identified by genetic screening (Figure S1B). MGL-Tg mice were viable and healthy, and displayed normal responses to a standard set of neuromuscular tests (Crawley, 2000). The CaMKIIα-MGL transgene produced robust MGL expression throughout the adult forebrain (Figures 1B and 1C), with a distribution pattern resembling that of CaMKIIα (Mayford et al., 1995; Casanova et al., 2001). Particularly high expression was noted in hippocampus and cortex, but significant levels were also seen in other regions (Figures 1B and 1C). Immunohistochemical analyses confirmed this distribution (Figure 2).

MGL-Tg Mice Have a Selective Deficit in Forebrain 2-AG

Consistent with protein expression, MGL activity was higher and 2-AG levels were lower in the forebrain of MGL-Tg mice, relative to wild-type controls (Figures 1D and 1E). Additional lipid analyses revealed that MGL over-expression preferentially altered 2-AG content, producing only a modest decrease in other 2-acyl-*sn*-glycerols (Table S1) and without altering anandamide, arachidonic acid (AA) (Figure 1F) or other fatty acids (Table S1). Moreover, there were no detectable changes in the transcription of various endocannabinoid-related genes (Figure 1G and S1C). MGL expression was unchanged in peripheral tissues of MGL-Tg mice, including sympathetic stellate ganglia (Figure 1H), and

normal MGL activity was found in spleen and BAT, which are densely innervated by sympathetic fibers (Figure S2A and S2B). No alterations in 2-AG or AA were observed in a panel of peripheral tissues that included BAT, spleen and liver (Figure S2C and S2D). The results suggest that CaMKIIα-driven MGL over-expression accelerates 2-AG degradation and reduces 2-AG availability. Importantly, this effect is restricted to the forebrain and is not associated with overt changes in other components of the endocannabinoid system.

MGL-Tg Mice Are Lean, Hyperphagic and Hypoactive

Starting from 14 weeks of age, the body-weight trajectory of MGL-Tg mice diverged from that of their wild-type littermates. Transgenic animals showed reduced weight gain (Figure 3A), decreased adiposity (Figure 3B) and increased lean mass (Figure 3C) relative to controls. These differences in body composition were accompanied by lower plasma triglyceride levels (Figure 3D), decreased serum glucose levels (Figure 3E) and heightened glucose uptake (Figure 3F). By contrast, total body water (Figure 3G) and dietary fat absorption (Figure S3A) were identical in the two strains. Despite their reduced body weight, MGL-Tg mice fed more frequently (Figures 3H and S3B-S3D), ate a greater amount of food (Figure 3I) and moved less (Figure 3J) than did control mice. This unusual coexistence of leanness, increased feeding and reduced motor activity was the most prominent outward feature of MGL-Tg mutants.

MGL-Tg Mice are Resistant to Diet-Induced Obesity

To investigate this feature further, we exposed the mice to a high-fat diet (60 kcal% fat) for 10 weeks. Although wild-type and MGL-Tg mice consumed equal amounts of food (Figure S4), the former became obese whereas the latter gained only a modest amount of weight (Figures 4A–C), displaying markedly reduced feed efficiency (Figure 4D) and fat mass (Figure 4E and Table S2). In addition, MGL-Tg mice did not present any of the metabolic signs that typically accompany obesity, showing no evidence of liver steatosis (Figures 4F and 4G), insulin resistance (Figure 4H) or leptin resistance (Figure 4I). As seen with mice kept on standard chow, blood glucose and triglyceride levels in fat-fed transgenic mice were significantly lower than those found in controls (Figures 4J and 4K). A plausible interpretation of these results is that lowered forebrain 2-AG availability is associated with an increase in energy dissipation, which renders MGL-Tg mice resistant to obesity and metabolic syndrome.

MGL-Tg Mice Show High Energy Cost of Activity

Indirect calorimetry measurements showed no difference in average energy expenditure, respiratory quotient or oxygen consumption between MGL-Tg and wild-type mice (Figures S5A and S5B). A regression analysis of the calorimetry data revealed, however, that transgenic mice used a greater amount of energy for any given level of motor activity (Figures 5A and 5B). Additional tests showed that core body temperature (Figure 5C) and, particularly, thermogenic responses to pharmacological activation of β_3-adrenergic receptors (Figure 5D) were higher in transgenic mice than controls. Consistently, β_3-adrenergic receptor expression (Figure 5E) and mitochondrial complex I and III activity (Figure 5F) were elevated in MGL-Tg mice. These traits are consistent with a heightened energetic cost of motor activity resulting, at least in part, from enhanced thermogenesis.

Impaired 2-AG Signaling at CB_1 Receptors Underlies Enhanced Thermogenesis

To determine whether deficits in 2-AG signaling at CB_1 account for the abnormal thermoregulation observed in MGL-Tg mice, we treated the animals with a single dose of the irreversible MGL inhibitor JZL184 (Long et al., 2009a) and measured baseline and β_3-adrenergic-induced thermogenesis 6 h later. As expected (Long et al., 2009b), JZL184

inhibited brain MGL activity (Figure S6A) and increased brain 2-AG levels (Figure S6B), without affecting DGL activity (Figure S6C). Moreover, JZL184 caused a modest hypothermia in both strains (Figure S6D). However, the most notable consequence of MGL blockade was a normalization of the thermogenic response to β_3-receptor activation in transgenic mice (Figure 5D). This effect was reversed by the CB_1 inverse agonist rimonabant, providing evidence that it resulted from restoration of 2-AG signaling at CB_1 (Figure 5D). Furthermore, rimonabant enhanced β_3-adrenergic-induced hyperthermia in wild-type mice (Figure 5D), which is suggestive of an intrinsic endocannabinoid modulation of thermogenesis (Long et al., 2009b). JZL184 did not normalize other phenotypic changes observed in MGL-Tg mice, including plasma levels of glucose, insulin and leptin, or body weight (Figure S6E and S6F). Collectively, the results suggest that 2-AG signaling at CB_1 regulates the activity of forebrain circuits that control energy dissipation.

Increased Mitochondrial Density in BAT

We next asked whether alterations in the morphology of BAT mitochondria may account for the increased thermogenic response observed in MGL-Tg mice. Electron microscopy studies showed that the mitochondrial to cytoplasmic area ratio was higher in MGL-Tg mice than controls ($p = 0.0292$; Figure 6A and 6B). This difference was likely due to changes in mitochondrial area and density (Figure S7A and S7B). Additional investigations showed that uncoupling protein-1 (UCP1) (Figure 6C and 6D) and type 2 iodothyronine deiodinase (Figure S7C) were elevated in BAT of transgenic mice, confirming the presence of a heightened thermogenic capacity in these mutants.

Changes in CART Expression in Hypothalamus

To identify neural circuits that might be modified by MGL over-expression, we surveyed the hypothalamus of transgenic mice for quantitative changes in a set of 42 mRNAs encoding for proteins known to participate in systemic metabolism. Among the transcripts targeted by our analysis (Table S3), only that encoding for the neuropeptide CART showed statistically detectable elevations in MGL-Tg mice (Table S4). There was a trend to higher *Pomc* mRNA content, but this failed to reach statistical significance ($p = 0.063$; Table S4). By contrast, the transcription of other genes involved in energy homeostasis – including leptin receptor and agouti-related peptide – was similar between transgenic and control animals (Table S4). Quantitative RT-PCR and western blot analyses confirmed that CART expression was markedly elevated in the hypothalamus, but not in several other brain regions of MGL-Tg mice (Figure 7A and 7B). In agreement with the known localization of CART-expressing neurons (Gautvik et al., 1996; Fekete et al., 2006), *in situ* hybridization and immunohistochemistry experiments identified the arcuate nucleus and dorsomedial hypothalamus as sites of enhanced CART mRNA transcription (Figure 7C), and the paraventricular nucleus as a site of increased CART peptide localization (Figure 7D). These findings suggest that CART expression is increased in MGL-Tg mice.

DISCUSSION

The present report describes the phenotype of transgenic mice that over-express MGL in forebrain neurons. The mutation causes a widespread reduction in forebrain 2-AG levels along with a series of behavioral and metabolic traits that are suggestive of excessive heat production. Compared to their wild-type littermates, MGL-Tg mice are lean, hyperphagic, resistant to diet-induced obesity, hyperthermic, and hypersensitive to β_3-adrenergic-stimulated thermogenesis. The latter abnormality is corrected by pharmacological blockade of MGL activity, which restores the ability of endogenous 2-AG to engage CB_1 receptors. Collectively, the results indicate that central 2-AG signaling at CB_1 regulates energy balance by controlling heat dissipation.

2-AG is considered the main endocannabinoid mediator of retrograde signaling at CNS synapses (Katona and Freund, 2008). Experiments in brain slices have suggested that activation of postsynaptic DGL-α releases 2-AG (Jung et al., 2005), which then diffuses across the synapse to ligate CB_1 receptors on axon terminals (Katona and Freund, 2008). These experiments do not clarify, however, the functions of 2-AG in live animals. Two genetic models have been developed to fill this knowledge gap. Deletion of DGL-α lowers brain 2-AG levels and suppresses endocannabinoid signaling in the mouse hippocampus (Tanimura et al., 2010; Gao et al., 2010), but also alters the steady-state levels of two endocannabinoid-related lipids: anandamide and arachidonic acid (Gao et al., 2010). On the other hand, MGL deletion causes 2-AG to accumulate in the mouse brain, which results in CB_1 receptor desensitization and tolerance to the effects of cannabinoid agonists (Chanda et al., 2010; Schlosburg et al., 2010). Because of these compensatory events, DGL-α- and MGL-null mice do not provide definitive insights on the roles played by 2-AG *in vivo*. Pharmacological approaches aimed at inhibiting DGL-α or MGL also suffer from various limitations, including inadequate target selectivity (Hoover et al., 2008) and dose-dependent CB_1 receptor desensitization (Schlosburg et al., 2010; Busquets-Garcia et al., 2011; Sciolino et al., 2011). Here, we utilized the CaMKIIα promoter to drive MGL expression in forebrain neurons (Mayford et al., 1995; Mayford et al., 1997). This allowed us to generate mice in which MGL activity is enhanced in the forebrain, but not cerebellum, sympathetic ganglia or peripheral organs. Importantly, the resulting decrement in 2-AG availability does not trigger compensatory mechanisms such as those observed in mice that do not express DGL-α or MGL (Chanda et al., 2010; Schlosburg et al., 2010). The reasons for this apparent lack of compensation are unclear, but might relate to the late developmental activation of the CaMKIIα promoter (Kojima et al., 1997; Mayford et al., 1997) or the presence of residual 2-AG levels in MGL-Tg mice. Thus, the first main result of our study is the generation of an animal model in which a selective deficiency in central 2-AG signaling can be unequivocally linked to alterations in phenotype.

We identified four sets of phenotypic changes that differentiate MGL-Tg mice from their wild-type littermates. First, MGL-Tg mice eat more and move less than do control animals. Second, irrespective of whether they are fed a normal or high-fat diet, MGL-Tg mice are resistant to body-weight gain, and their blood glucose and triglyceride levels are lower than those of wild-type controls. Third, MGL-Tg mice are strikingly hypersensitive to the thermogenic effects of β_3-adrenergic activation. Fourth, the BAT of MGL-Tg mice displays higher mitochondrial density and expression of proteins involved of non-shivering thermogenesis (Silva, 2006). Additionally, experiments with the MGL inhibitor JZL184 (Long et al., 2009a) showed that reinstating intrinsic 2-AG activity at CB_1 receptors normalizes β_3-adrenergic-dependent thermogenesis in MGL-Tg mice. These findings provide evidence that forebrain 2-AG signaling through CB_1 helps conserve body energy by quenching heat production. Supporting an energy-sparing role for central 2-AG, conditional mutant mice that lack CB_1 receptors in the forebrain and express fewer CB_1 receptors in sympathetic neurons were also shown to be hyperthermic, lean and resistant to diet-induced obesity (Quarta et al., 2010). As 2-AG is a mediator of retrograde synaptic transmission throughout the CNS (Katona and Freund, 2008), it is likely that 2-AG signaling at more than one forebrain site contributes to metabolic control. This is an important area for future investigation.

In conclusion, the present report introduces MGL-Tg mice as a new model to investigate the functions of central 2-AG-mediated endocannabinoid signaling. The phenotypic changes displayed by these mice suggest that 2-AG acting at brain CB_1 receptors may help to conserve body energy by moderating heat dissipation. These effects appear to be synergic with those exerted by CB_1 receptors in peripheral tissues (Kunos and Tam, 2011), further underscoring the pervasive roles of endocannabinoid signaling in energy metabolism.

EXPERIMENTAL PROCEDURES

Transgene Construction

We constructed the MGL transgene expression vector by inserting a 1.0-kb rat MGL-V5 polymerase chain reaction (PCR) product into the BamHI site of pNN265. The 2.5-kb NotI fragment of the plasmid, which encodes MGL-V5, 5′- and 3′-intron and poly A signal from SV40 (Choi et al., 1991), was then inserted into the pMM403 vector containing a 8.5-kb CaMKIIα promoter sequence (Mayford et al., 1995) to generate the pMM403-MGL construct, the identity of which was verified by DNA sequencing. MGL expression and enzyme activity were assessed after transfection of Chinese hamster ovary (CHO) cells with pNN265-MGL (Figure S1A).

Transgenic Mice

We prepared an 11-kb linearized DNA containing the CaMKIIα promoter and the MGL transgene by digestion of pMM403-MGL with SfiI. Transgenic founders were generated by pronuclear injection of linearized DNA into C57BL6/J zygotes (Transgenic Mouse Facility, University of California, Irvine), and male chimeras were crossed with C57BL6/J females. Animals were kept at 22 °C on a 12 h light/dark cycle, with free access to water and chow (Prolab RMH 2500; PMI Nutrition International, Brentwood, MO). We used male mice aged between 17 to 30 weeks under normal chow feeding, unless indicated otherwise. All procedures met the National Institutes of Health Guidelines for the Care and Use of Laboratory Animals, and were approved by the Institutional Animal Care and Use Committee of the University of California, Irvine.

Quantitative PCR

We performed quantitative real-time PCR as detailed elsewhere (Jung et al., 2011). Primers and fluorogenic probes were synthesized by TIB Molbiol (Adelphia, NJ) or purchased from Applied Biosystems (TaqMan(R) Gene Expression Assays, Foster City, CA) (Table S5).

Protein Measurements

Western blot analyses were conducted as described (Jung et al., 2011).

Lipid Analyses

Lipid extraction and analysis by liquid chromatography/mass spectrometry were conducted as described (Astarita et al., 2009).

MGL Activity Assays

Enzyme assays were conducted as described (Jung et al., 2011).

Immunohistochemistry

We perfused mice through their left heart ventricle with isotonic saline, and then with a solution containing 4% paraformaldehyde in 0.1 M phosphate buffer (PB, pH 7.2). Brains were collected, postfixed for 1 day in the fixation solution, and cut in coronal sections with a cryostat (20 μm thickness). The sections were treated with 0.3% hydrogen peroxide for 20 min and exposed to 3% normal goat serum for 1 h at room temperature. Sections were incubated overnight at 4°C with an MGL antibody (1:500, Dinh et al., 2002) or a CART antibody (1:1000, Phoenix Pharmaceuticals, Burlingame, CA), rinsed in 0.1 M PB and exposed to anti-mouse IgG conjugated with Alexa Fluor 488 (1:1000, Invitrogen, Carlsbad, CA) for 1 h. 4′-6-Diamidino-2-phenylindole (DAPI)-containing medium (Vector Laboratories, Burlingame, CA) was used for nucleus staining. For 3,3′-diaminobenzidine

(DAB) staining, the sections were washed after primary antibody incubation, and exposed to biotinylated goat anti-rabbit IgG (1:500, Vector Laboratories) for 1 h. After a 10-min rinse with 0.1 M PB, sections were treated with avidin–biotin–peroxidase complex (ABC, 1:200, Vector Laboratories) and developed with DAB with metal enhancer (Sigma-Aldrich, St. Louis, MO). Slides were rinsed, dehydrated in ascending ethanol concentrations, cleared in xylene and mounted with Eukitt mounting medium (Sigma-Aldrich). Images were captured using an Eclipse E600 microscope (Nikon, Tokyo, Japan).

Morphometric Analyses

Light microscopy and immunohistochemistry—BAT pieces were fixed overnight at 4°C in 4% paraformaldehyde in 0.1 M PB at pH 7.4. They were dehydrated, cleared and paraffin-embedded. Sections from 3 different levels (100 μm apart) were stained with hematoxilin-eosin for immunohistochemistry. UCP1 immunoreactivity was examined as follows. For each section level, 3-μm-thick dewaxed sections were incubated with sheep anti-UCP1 (1:6000, kindly provided by Daniel Ricquier, Université Paris Descartes, France) according to the avidin-biotin complex (ABC) method, as follows: 1) endogenous peroxidase blocking with 3% hydrogen peroxide in methanol; 2) normal rabbit serum (1:75) for 20 min to reduce nonspecific background; 3) incubation with primary antibodies against UCP1 overnight at 4°C; 4) rabbit anti-sheep IgG biotin conjugated (1:200; Vector Laboratories); 5) ABC kit (Vector Labs); 6) enzymatic reaction to reveal peroxidase with Sigma Fast 3,3′-diaminobenzidine (Sigma-Aldrich) as substrate. Finally, sections were counterstained with hematoxilin and mounted in Eukitt (Fluka, Deisenhofen, Germany). Images were captured with a Nikon Eclipse 80i light microscope (Nikon).

Electron Microscopy—Immediately after removal, small tissue fragments were fixed in 2% glutaraldehyde-2% paraformaldehyde in 0.1 M PB (pH 7.4) for 4 h, postfixed in 1% osmium tetroxide, and embedded in an Epon-Araldite mixture. Semithin sections (2 μm) were stained with toluidine blue. Thin sections were obtained with an MT-X ultratome (RMC, Tucson, AZ, USA), stained with lead citrate, and examined with a CM10 transmission electron microscope (Philips, Eindhoven, The Netherlands).

Body Composition

Fat mass and lean mass were measured in freely moving mice using ^{1}H magnetic resonance spectroscopy (EchoMRI-100; Echomedical Systems, Houston, TX), and expressed as percentage of total body mass. Measurements for each mouse were performed in triplicate and the average of three replicates was used for statistical purposes. In the diet-induced obesity experiment, weights of individual organs and fat pads were measured after dissection.

Blood Chemistry

Blood analyses were performed using plasma from 18-week old mice, unless indicated otherwise. Glucose and triglyceride levels were quantified in triplicate using colorimetric assays (Cayman Chemical, Ann Arbor, MI). Insulin and leptin levels were determined in duplicate by enzyme-linked immunosorbent assays (ELISA) (Millipore, Billerica, MA). For glucose tolerance tests, 17 to 18-week old mice were food-deprived for 4 h and glucose (2 mg/g) was administered by intraperitoneal injection. Blood was taken from the tail at 0, 30, 60 and 150 min after injection and glucose levels were measured in serum.

Feeding Behavior

Food intake was recorded in free-feeding mice using an automated monitoring system (Scipro, New York, NY) as described (Gaetani et al., 2003). Meal analysis was performed

adopting a minimum inter-response interval separating two meals of 10 min. The following feeding parameters were analyzed: total food intake during 24 h (g/kg); feeding latency (min); meal size (g/kg); eating rate [(g/kg)/min]; and meal frequency (meals/h).

Diet-Induced Obesity

Wild-type and MGL-Tg mice (20-week old) were single-housed (22 °C on a 12 h light/dark cycle) and kept for 10 weeks on a high-fat diet (60 kcal % fat, Research Diets, Inc., New Brunswick, NJ) with free access to water. At the end of the experiment, animals were food-deprived for 4 h and killed.

Metabolic Chamber Recordings

Adult mice were acclimated to metabolic chambers (TSE Systems, Germany) for 3 days before beginning the recordings. Energy expenditure, respiratory exchange ratio, food intake, water intake and locomotor activity (in X and Z axis) were measured simultaneously over a 24-h period for 2 consecutive days. VO_2, VCO_2 and energy expenditure were calculated following manufacturer's guidelines (PhenoMaster Software, TSE Systems).

Motor Activity

The TSE Indirect Calorimetry System was customized to include a multidimensional light beam and light sensor system. The parallel beams were set up close enough so that no mouse could be in the calorimeter cage without at least 1 light beam being broken by its body. The motor activity–monitoring software of this system was programmed to interpret breaking of consecutive beams of the lower level of the beam grid to indicate ambulatory movement. Recorded breaks of light beams within a second beam grid located in the upper half of the home cage would be interpreted as rearing behavior, which often correlates with feeding from hanging feeders or climbing activities. Finally, rapid consecutive breaks and reconnection of the same light beams were interpreted as stationary motor activity or fidgeting. The recordings of such events were used to indicate shivering or fidgeting.

Temperature Measurements

Adult mice were food-restricted overnight and anesthetized by intraperitoneal injection of ketamine/xylazine. The mice were placed on a heating pad kept at 30 °C while core temperature was monitored using a rectal thermometer. After 20-min, the β_3-adrenergic agonist CL-316243 (0.1 mg/kg, dissolved in saline) (Tocris Bioscience, Ellisville, MO) was administered by intraperitoneal injection. Body temperature was recorded every min for 40 min. JZL184 (16 mg/kg, dissolved in 80% polyethylene glycol 200, 20% Tween-80) (Cayman Chemical) was administered 6 h before CL-316243 and rimonabant (10 mg/kg, dissolved in 5% polyethylene glycol 200, 5% Tween-80 in saline) (RTI International, Research Triangle Park, NC) was administered 15 min before JZL184.

Mitochondrial Activity

Interscapular BAT was isolated after 6 h from intraperitoneal injection of CL-316243 (0.1 mg/kg) or saline and homogenized in 2 ml of ice-cold buffer containing MOPS (10 mM, pH 7.2), mannitol (225 mM), sucrose (75 mM), EGTA (1 mM), and 0.5% BSA. Homogenates were centrifuged at 600 × g for 10 min at 4 °C, and supernatants centrifuged again at 7,000 × g for 10 min at 4°C. Mitochondria-enriched pellets were suspended in a hypotonic medium and freeze-thawed 3 times. NADH-cytochrome c oxidoreductase activity by Complex I and III was determined in an assay buffer containing Tris-HCl (50 mM, pH 8.0), BSA (5 mg/ml), oxidized cytochrome c (40 μM), and potassium cyanide (0.24 mM). Reactions were initiated by addition of NADH (0.8 mM) and absorbance at 550 nm was measured 3 min later to quantify cytochrome c reduction (Díaz et al., 2009).

In situ Hybridization

We prepared riboprobes ([^{35}S]-cRNA) for *Cartpt* (coding region 1–390 of mouse CART) using RNA polymerase (Roche, Indianapolis, IN) in the presence of [^{35}S]-UTP. Coronal brain sections (20 μm thickness) were cut on a cryostat (Microm-Thermo Scientific, Germany) and hybridized at 60°C for 16 h in buffer containing [^{35}S]-cRNA (75×10^6 dpm/ml), 10% dextran sulfate, 50% formamide, 1xDenhardt's solution, 100 μg/ml denatured salmon sperm DNA, 0.15 mg/ml tRNA and 40 mM dithiothreitol. After hybridization, the sections were washed in gradient SSC solutions (4xSSC, 2x SSC, 1xSSC, and 0.1xSSC), and exposed to Kodak Biomax film (Sigma-Aldrich) for 72 h. The specificity of the hybridization signal was ascertained by hybridization of the same sections labeled with sense probes.

Statistical Analyses

Results are expressed as means ± SEM. Significance was determined using two-tailed Student's *t*-test or two-way analysis of variance (ANOVA) with Bonferroni post-test, as appropriate, and differences were considered significant if $p<0.05$. Analyses were conducted using GraphPad Prism (GraphPad Software, San Diego, CA).

Supplementary Material

Refer to Web version on PubMed Central for supplementary material.

Acknowledgments

This work was supported by a grant (RO1 DA-012447) from the National Institute on Drug Abuse (to D.P.). The contribution of the Agilent Technologies/University of California, Irvine Analytical Discovery Facility, Center for Drug Discovery is gratefully acknowledged. The authors declare no actual or potential conflicts of interest.

References

Abbott CR, Rossi M, Wren AM, Murphy KG, Kennedy AR, Stanley SA, Zollner AN, Morgan DG, Morgan I, Ghatei MA, Small CJ, Bloom SR. Evidence of an orexigenic role for cocaine- and amphetamine-regulated transcript after administration into discrete hypothalamic nuclei. Endocrinology. 2001; 142:3457–3463. [PubMed: 11459791]

Astarita G, Piomelli D. Lipidomic analysis of endocannabinoid metabolism in biological samples. J Chromatogr B Analyt Technol Biomed Life Sci. 2009; 877:2755–2767.

Bajzer M, Olivieri M, Haas MK, Pfluger PT, Magrisso IJ, Foster MT, Tschöp MH, Krawczewski-Carhuatanta KA, Cota D, Obici S. Cannabinoid receptor 1 (CB1) antagonism enhances glucose utilisation and activates brown adipose tissue in diet-induced obese mice. Diabetologia. 2011; 54:3121–3131. [PubMed: 21987346]

Blankman JL, Simon GM, Cravatt BF. A comprehensive profile of brain enzymes that hydrolyze the endocannabinoid 2-arachidonoylglycerol. Chem Biol. 2007; 14:1347–1356. [PubMed: 18096503]

Busquets-Garcia A, Puighermanal E, Pastor A, de la Torre R, Maldonado R, Ozaita A. Differential role of anandamide and 2-arachidonoylglycerol in memory and anxiety-like responses. Biol Psychiatry. 2011; 70:479–486. [PubMed: 21684528]

Casanova E, Fehsenfeld S, Mantamadiotis T, Lemberger T, Greiner E, Stewart AF, Schütz G. A CamKIIalpha iCre BAC allows brain-specific gene inactivation. Genesis. 2001; 31:37–42. [PubMed: 11668676]

Chanda PK, Gao Y, Mark L, Btesh J, Strassle BW, Lu P, Piesla MJ, Zhang MY, Bingham B, Uveges A, Kowal D, Garbe D, Kouranova EV, Ring RH, Bates B, Pangalos MN, Kennedy JD, Whiteside GT, Samad TA. Monoacylglycerol lipase activity is a critical modulator of the tone and integrity of the endocannabinoid system. Mol Pharmacol. 2010; 78:996–1003. [PubMed: 20855465]

Choi T, Huang M, Gorman C, Jaenisch R. A generic intron increases gene expression in transgenic mice. Mol Cell Biol. 1991; 11:3070–3074. [PubMed: 2038318]

Cota D, Marsicano G, Tschöp M, Grübler Y, Flachskamm C, Schubert M, Auer D, Yassouridis A, Thöne-Reineke C, Ortmann S, Tomassoni F, Cervino C, Nisoli E, Linthorst AC, Pasquali R, Lutz B, Stalla GK, Pagotto U. The endogenous cannabinoid system affects energy balance via central orexigenic drive and peripheral lipogenesis. J Clin Invest. 2003; 112:423–431. [PubMed: 12897210]

Crawley, JN. What's Wrong With My Mouse? Behavioral Phenotyping of Transgenic and Knockout Mice. New York: Wiley-Liss; 2000.

Díaz F, Barrientos A, Fontanesi F. Evaluation of the mitochondrial respiratory chain and oxidative phosphorylation system using blue native gel electrophoresis. Curr Protoc Hum Genet. 2009 Oct. (Unit 19.4)

Di Marzo V, Goparaju SK, Wang L, Liu J, Bátkai S, Járai Z, Fezza F, Miura GI, Palmiter RD, Sugiura T, Kunos G. Leptin-regulated endocannabinoids are involved in maintaining food intake. Nature. 2001; 410:822–825. [PubMed: 11298451]

Dinh TP, Carpenter D, Leslie FM, Freund TF, Katona I, Sensi SL, Kathuria S, Piomelli D. Brain monoglyceride lipase participating in endocannabinoid inactivation. Proc Natl Acad Sci U S A. 2002; 99:10819–10824. [PubMed: 12136125]

Eckardt K, Sell H, Taube A, Koenen M, Platzbecker B, Cramer A, Horrighs A, Lehtonen M, Tennagels N, Eckel J. Cannabinoid type 1 receptors in human skeletal muscle cells participate in the negative crosstalk between fat and muscle. Diabetologia. 2009; 52:664–674. [PubMed: 19089403]

Elmquist JK. Hypothalamic pathways underlying the endocrine, autonomic, and behavioral effects of leptin. Int J Obes Relat Metab Disord. 2001; 25 (Suppl 5):S78–82. [PubMed: 11840221]

Engeli S, Böhnke J, Feldpausch M, Gorzelniak K, Janke J, Bátkai S, Pacher P, Harvey-White J, Luft FC, Sharma AM, Jordan J. Activation of the peripheral endocannabinoid system in human obesity. Diabetes. 2005; 54:2838–2843. [PubMed: 16186383]

Fekete C, Lechan RM. Neuroendocrine implications for the association between cocaine- and amphetamine regulated transcript (CART) and hypophysiotropic thyrotropin-releasing hormone (TRH). Peptides. 2006; 27:2012–2018. [PubMed: 16730860]

Gaetani S, Oveisi F, Piomelli D. Modulation of meal pattern in the rat by the anorexic lipid mediator oleoylethanolamide. Neuropsychopharmacology. 2003; 28:1311–1316. [PubMed: 12700681]

Gao Y, Vasilyev DV, Goncalves MB, Howell FV, Hobbs C, Reisenberg M, Shen R, Zhang MY, Strassle BW, Lu P, Mark L, Piesla MJ, Deng K, Kouranova EV, Ring RH, Whiteside GT, Bates B, Walsh FS, Williams G, Pangalos MN, Samad TA, Doherty P. Loss of retrograde endocannabinoid signaling and reduced adult neurogenesis in diacylglycerol lipase knock-out mice. J Neurosci. 2010; 30:2017–2024. [PubMed: 20147530]

Gautvik KM, de Lecea L, Gautvik VT, Danielson PE, Tranque P, Dopazo A, Bloom FE, Sutcliffe JG. Overview of the most prevalent hypothalamus-specific mRNAs, as identified by directional tag PCR subtraction. Proc Natl Acad Sci U S A. 1996; 93:8733–8738. [PubMed: 8710940]

Gómez R, Navarro M, Ferrer B, Trigo JM, Bilbao A, Del Arco I, Cippitelli A, Nava F, Piomelli D, Rodríguez de Fonseca F. A peripheral mechanism for CB1 cannabinoid receptor-dependent modulation of feeding. J Neurosci. 2002; 22:9612–9617. [PubMed: 12417686]

Gulyas AI, Cravatt BF, Bracey MH, Dinh TP, Piomelli D, Boscia F, Freund TF. Segregation of two endocannabinoid-hydrolyzing enzymes into pre- and postsynaptic compartments in the rat hippocampus, cerebellum and amygdala. Eur J Neurosci. 2004; 20:441–458. [PubMed: 15233753]

Hashimotodani Y, Ohno-Shosaku T, Tsubokawa H, Ogata H, Emoto K, Maejima T, Araishi K, Shin HS, Kano M. Phospholipase Cbeta serves as a coincidence detector through its Ca2+ dependency for triggering retrograde endocannabinoid signal. Neuron. 2005; 45:257–268. [PubMed: 15664177]

Hentges ST, Low MJ, Williams JT. Differential regulation of synaptic inputs by constitutively released endocannabinoids and exogenous cannabinoids. J Neurosci. 2005; 25:9746–9751. [PubMed: 16237178]

Herling AW, Kilp S, Juretschke HP, Neumann-Haefelin C, Gerl M, Kramer W. Reversal of visceral adiposity in candy-diet fed female Wistar rats by the CB1 receptor antagonist rimonabant. Int J Obes (Lond). 2008; 32:1363–1372. [PubMed: 18626484]

Hoover HS, Blankman JL, Niessen S, Cravatt BF. Selectivity of inhibitors of endocannabinoid biosynthesis evaluated by activity-based protein profiling. Bioorg Med Chem Lett. 2008; 18:5838–5841. [PubMed: 18657971]

Ioannides-Demos LL, Piccenna L, McNeil JJ. Pharmacotherapies for obesity: past, current, and future therapies. J Obes. 2011; 2011:179674. [PubMed: 21197148]

Jung KM, Mangieri R, Stapleton C, Kim J, Fegley D, Wallace M, Mackie K, Piomelli D. Stimulation of endocannabinoid formation in brain slice cultures through activation of group I metabotropic glutamate receptors. Mol Pharmacol. 2005; 68:1196–1202. [PubMed: 16051747]

Jung KM, Astarita G, Thongkham D, Piomelli D. Diacylglycerol lipase-alpha and -beta control neurite outgrowth in neuro-2a cells through distinct molecular mechanisms. Mol Pharmacol. 2011; 80:60–67. [PubMed: 21493725]

Katona I, Freund TF. Endocannabinoid signaling as a synaptic circuit breaker in neurological disease. Nat Med. 2008; 14:923–930. [PubMed: 18776886]

Kirkham TC. Cannabinoids and appetite: food craving and food pleasure. Int Rev Psychiatry. 2009; 21:163–171. [PubMed: 19367510]

Kojima N, Wang J, Mansuy IM, Grant SG, Mayford M, Kandel ER. Rescuing impairment of long-term potentiation in fyn-deficient mice by introducing Fyn transgene. Proc Natl Acad Sci U S A. 1997; 94:4761–4765. [PubMed: 9114065]

Kola B, Farkas I, Christ-Crain M, Wittmann G, Lolli F, Amin F, Harvey-White J, Liposits Z, Kunos G, Grossman AB, Fekete C, Korbonits M. The orexigenic effect of ghrelin is mediated through central activation of the endogenous cannabinoid system. PLoS One. 2008; 3:e1797. [PubMed: 18335063]

Kong WM, Stanley S, Gardiner J, Abbott C, Murphy K, Seth A, Connoley I, Ghatei M, Stephens D, Bloom S. A role for arcuate cocaine and amphetamine-regulated transcript in hyperphagia, thermogenesis, and cold adaptation. FASEB J. 2003; 17:1688–1690. [PubMed: 12958177]

Kunos G, Tam J. The case for peripheral CB(1) receptor blockade in the treatment of visceral obesity and its cardiometabolic complications. Br J Pharmacol. 2011; 163:1423–1431. [PubMed: 21434882]

Long JZ, Nomura DK, Cravatt BF. Characterization of monoacylglycerol lipase inhibition reveals differences in central and peripheral endocannabinoid metabolism. Chem Biol. 2009a; 16:744–753. [PubMed: 19635411]

Long JZ, Li W, Booker L, Burston JJ, Kinsey SG, Schlosburg JE, Pavón FJ, Serrano AM, Selley DE, Parsons LH, Lichtman AH, Cravatt BF. Selective blockade of 2-arachidonoylglycerol hydrolysis produces cannabinoid behavioral effects. Nat Chem Biol. 2009b; 5:37–44. [PubMed: 19029917]

LoVerme J, Duranti A, Tontini A, Spadoni G, Mor M, Rivara S, Stella N, Xu C, Tarzia G, Piomelli D. Synthesis and characterization of a peripherally restricted CB1 cannabinoid antagonist, URB447, that reduces feeding and body-weight gain in mice. Bioorg Med Chem Lett. 2009; 19:639–643. [PubMed: 19128970]

Mackie K. Cannabinoid receptors as therapeutic targets. Annu Rev Pharmacol Toxicol. 2006; 46:101–122. [PubMed: 16402900]

Mancini, G.; Quarta, C.; Srivastava, RK.; Klaus, S.; Pagotto, U.; Lutz, B. Adipocyte-specific CB1 conditional knock-out mice: new insights in the study of obesity and metabolic syndrome. 20th Annual Symposium on the Cannabinoids; Research Triangle Park, NC. International Cannabinoid Research Society; 2010. p. 17

Marrs WR, Blankman JL, Horne EA, Thomazeau A, Lin YH, Coy J, Bodor AL, Muccioli GG, Hu SS, Woodruff G, Fung S, Lafourcade M, Alexander JP, Long JZ, Li W, Xu C, Möller T, Mackie K, Manzoni OJ, Cravatt BF, Stella N. The serine hydrolase ABHD6 controls the accumulation and efficacy of 2-AG at cannabinoid receptors. Nat Neurosci. 2010; 13:951–957. [PubMed: 20657592]

Matias I, Di Marzo V. Endocannabinoids and the control of energy balance. Trends Endocrinol Metab. 2007; 18:27–37. [PubMed: 17141520]

Mayford M, Wang J, Kandel ER, O'Dell TJ. CaMKII regulates the frequency-response function of hippocampal synapses for the production of both LTD and LTP. Cell. 1995; 81:891–904. [PubMed: 7781066]

Mayford M, Mansuy IM, Muller RU, Kandel ER. Memory and behavior: a second generation of genetically modified mice. Curr Biol. 1997; 7:R580–589. [PubMed: 9285710]

Osei-Hyiaman D, DePetrillo M, Pacher P, Liu J, Radaeva S, Bátkai S, Harvey-White J, Mackie K, Offertáler L, Wang L, Kunos G. Endocannabinoid activation at hepatic CB1 receptors stimulates fatty acid synthesis and contributes to diet-induced obesity. J Clin Invest. 2005; 115:1298–1305. [PubMed: 15864349]

Osei-Hyiaman D, Liu J, Zhou L, Godlewski G, Harvey-White J, Jeong WI, Bátkai S, Marsicano G, Lutz B, Buettner C, Kunos G. Hepatic CB1 receptor is required for development of diet-induced steatosis, dyslipidemia, and insulin and leptin resistance in mice. J Clin Invest. 2008; 118:3160–3169. [PubMed: 18677409]

Piomelli D, Astarita G, Rapaka R. A neuroscientist's guide to lipidomics. Nat Rev Neurosci. 2007; 8:743–754. [PubMed: 17882252]

Quarta C, Bellocchio L, Mancini G, Mazza R, Cervino C, Braulke LJ, Fekete C, Latorre R, Nanni C, Bucci M, Clemens LE, Heldmaier G, Watanabe M, Leste-Lassere T, Maitre M, Tedesco L, Fanelli F, Reuss S, Klaus S, Srivastava RK, Monory K, Valerio A, Grandis A, De Giorgio R, Pasquali R, Nisoli E, Cota D, Lutz B, Marsicano G, Pagotto U. CB(1) signaling in forebrain and sympathetic neurons is a key determinant of endocannabinoid actions on energy balance. Cell Metab. 2010; 11:273–285. [PubMed: 20374960]

Schlosburg JE, Blankman JL, Long JZ, Nomura DK, Pan B, Kinsey SG, Nguyen PT, Ramesh D, Booker L, Burston JJ, Thomas EA, Selley DE, Sim-Selley LJ, Liu QS, Lichtman AH, Cravatt BF. Chronic monoacylglycerol lipase blockade causes functional antagonism of the endocannabinoid system. Nat Neurosci. 2010; 13:1113–1119. [PubMed: 20729846]

Sciolino NR, Zhou W, Hohmann AG. Enhancement of endocannabinoid signaling with JZL184, an inhibitor of the 2-arachidonoylglycerol hydrolyzing enzyme monoacylglycerol lipase, produces anxiolytic effects under conditions of high environmental aversiveness in rats. Pharmacol Res. 2011; 64:226–234. [PubMed: 21600985]

Silva JE. Thermogenic mechanisms and their hormonal regulation. Physiol Rev. 2006; 86:435–464. [PubMed: 16601266]

Smith KL, Gardiner JV, Ward HL, Kong WM, Murphy KG, Martin NM, Ghatei MA, Bloom SR. Overexpression of CART in the PVN increases food intake and weight gain in rats. Obesity (Silver Spring). 2008; 16:2239–2244. [PubMed: 18719668]

Stella N, Schweitzer P, Piomelli D. A second endogenous cannabinoid that modulates long-term potentiation. Nature. 1997; 388:773–778. [PubMed: 9285589]

Tam J, Vemuri VK, Liu J, Bátkai S, Mukhopadhyay B, Godlewski G, Osei-Hyiaman D, Ohnuma S, Ambudkar SV, Pickel J, Makriyannis A, Kunos G. Peripheral CB1 cannabinoid receptor blockade improves cardiometabolic risk in mouse models of obesity. J Clin Invest. 2010; 120:2953–66. [PubMed: 20664173]

Tanimura A, Yamazaki M, Hashimotodani Y, Uchigashima M, Kawata S, Abe M, Kita Y, Hashimoto K, Shimizu T, Watanabe M, Sakimura K, Kano M. The endocannabinoid 2-arachidonoylglycerol produced by diacylglycerol lipase alpha mediates retrograde suppression of synaptic transmission. Neuron. 2010; 65:320–327. [PubMed: 20159446]

Tung YC, Rimmington D, O'Rahilly S, Coll AP. Pro-opiomelanocortin modulates the thermogenic and physical activity responses to high-fat feeding and markedly influences dietary fat preference. Endocrinology. 2007; 148:5331–5338. [PubMed: 17717049]

HIGHLIGHTS

- We developed transgenic mice that selectively over-express MGL in the forebrain
- The mice show an uncompensated deficit in forebrain 2-AG signaling
- They are lean, resistant to diet-induced obesity and have high energy cost of activity
- Their phenotype suggests a role for forebrain 2-AG in metabolic control

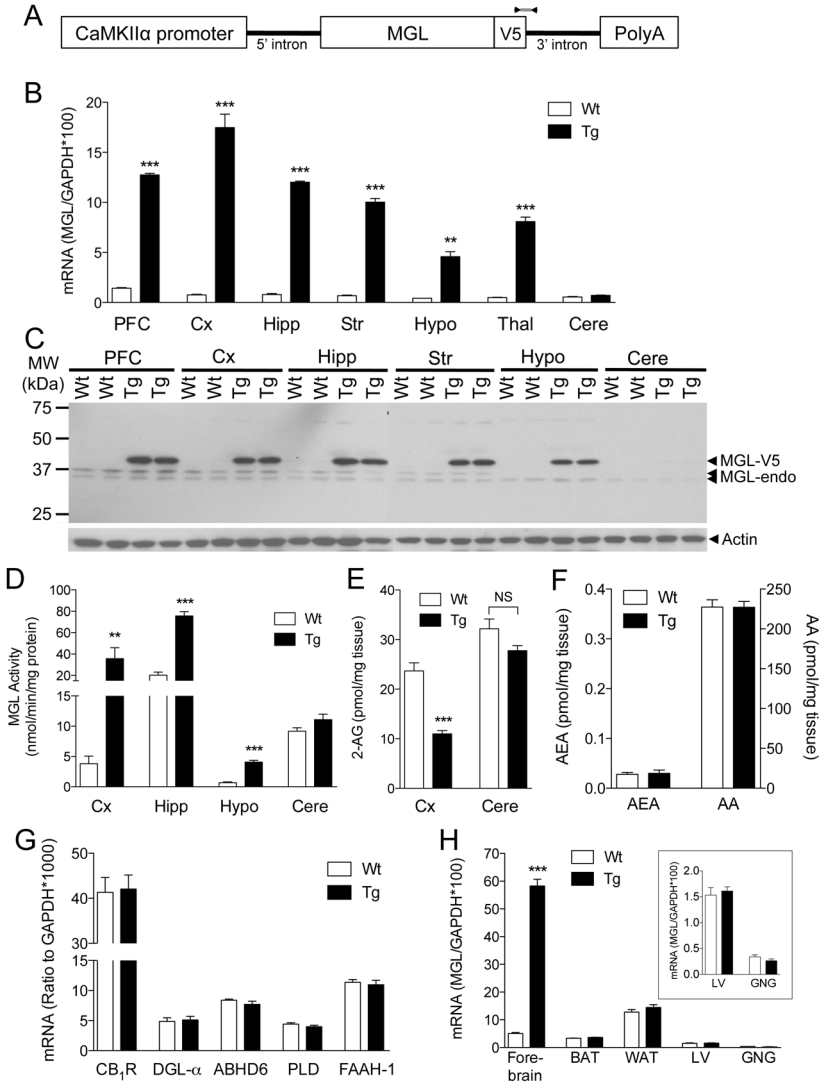

Figure 1. Biochemical characterization of MGL-Tg mice

(A) Schematic representation of the pMM403-CamKIIα-MGL-V5 construct utilized to generate MGL-Tg mice. The arrows indicate the position of the amplicon used for genotyping.

(B) MGL mRNA levels in brain regions of wild-type mice (open bars) or MGL-Tg mice (closed bars). PFC: prefrontal cortex; Cx, rest of the cortex; Hipp, hippocampus; Str, striatum; Hypo, hypothalamus; Thal, thalamus; Cere, cerebellum. Results are expressed as mean ± SEM. $^{**}p<0.01$ and $^{***}p<0.001$ (n=3).

(C) MGL protein levels in brain regions of wild-type (Wt) or MGL-Tg mice. Arrows indicate the apparent molecular weight (MW, in kDa) of the MGL-V5 transgene, endogenous MGL and actin (used as standard). The experiment was repeated twice with identical results.

(D) MGL activity and (E) 2-AG levels in various brain regions of wild-type (open bars) or MGL-Tg mice (closed bars). (F) anandamide (AEA) and arachidonic acid (AA) levels in the cortex. $^{**}p<0.01$ and $^{***}p<0.001$ (n=6–7).

(G) Levels of mRNAs encoding for CB_1 (CB_1R), diacylglycerol lipase-α (DGL-α), α-β-hydrolase domain 6 (ABHD6), *N*-acylphosphatidylethanolamine-specific phospholipase D

(NAPE-PLD) and fatty acid amide hydrolase-1 (FAAH-1) in the forebrain of wild-type (open bars) or MGL-Tg mice (closed bars) (n=5).
(H) MGL mRNA levels in various tissues of wild-type (open bars) or MGL-Tg mice (closed bars). Abbreviations: BAT, brown adipose tissue; WAT, white adipose tissue; LV, liver; GNG, sympathetic stellate ganglion. ***p<0.001 (n=3). The inset shows liver and GNG data in a magnified scale.

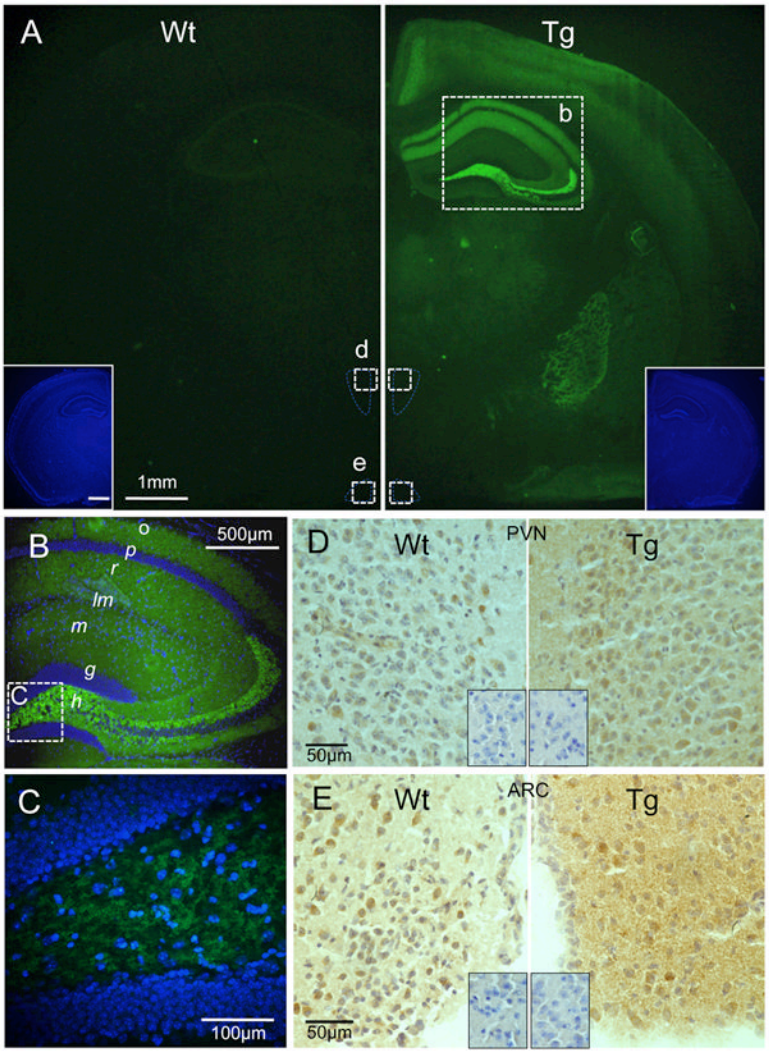

Figure 2. Neuroanatomical characterization of MGL-Tg mice

(A) Immunohistochemical localization of MGL in coronal brain sections from wild-type (Wt) and MGL-Tg (Tg) mice, using an antibody that recognizes both native and transgene-encoded MGL. The insets show nuclear staining with 4′,6-diamidino-2-phenylindole (DAPI). The dashed boxes marked b, d, and e highlight sections that are magnified in panel B–E.

(B–C) Immunohistochemical localization of MGL in hippocampus of MGL-Tg mice. A laminar, punctuated immunostaining pattern (green) is observed in the stratum oriens (o), stratum radiatum (r), hilus (h) and stratum moleculare (m) of the dentate gyrus. Other abbreviations: *p*, stratum pyramidale; *lm*, stratum lacunosum-moleculare; *g*, stratum granulosum. DAPI staining is shown in blue.

(D–E) Immunohistochemical localization of MGL in the paraventricular (PVN, D) and arcuate nuclei (ARC, E) of the hypothalamus in wild-type (Wt) and MGL-Tg (Tg) mice (dashed boxes d and e in panel A). The insets in D and E show negative control staining of adjacent slides using antibody pre-absorbed with purified MGL (0.18 mg/ml).

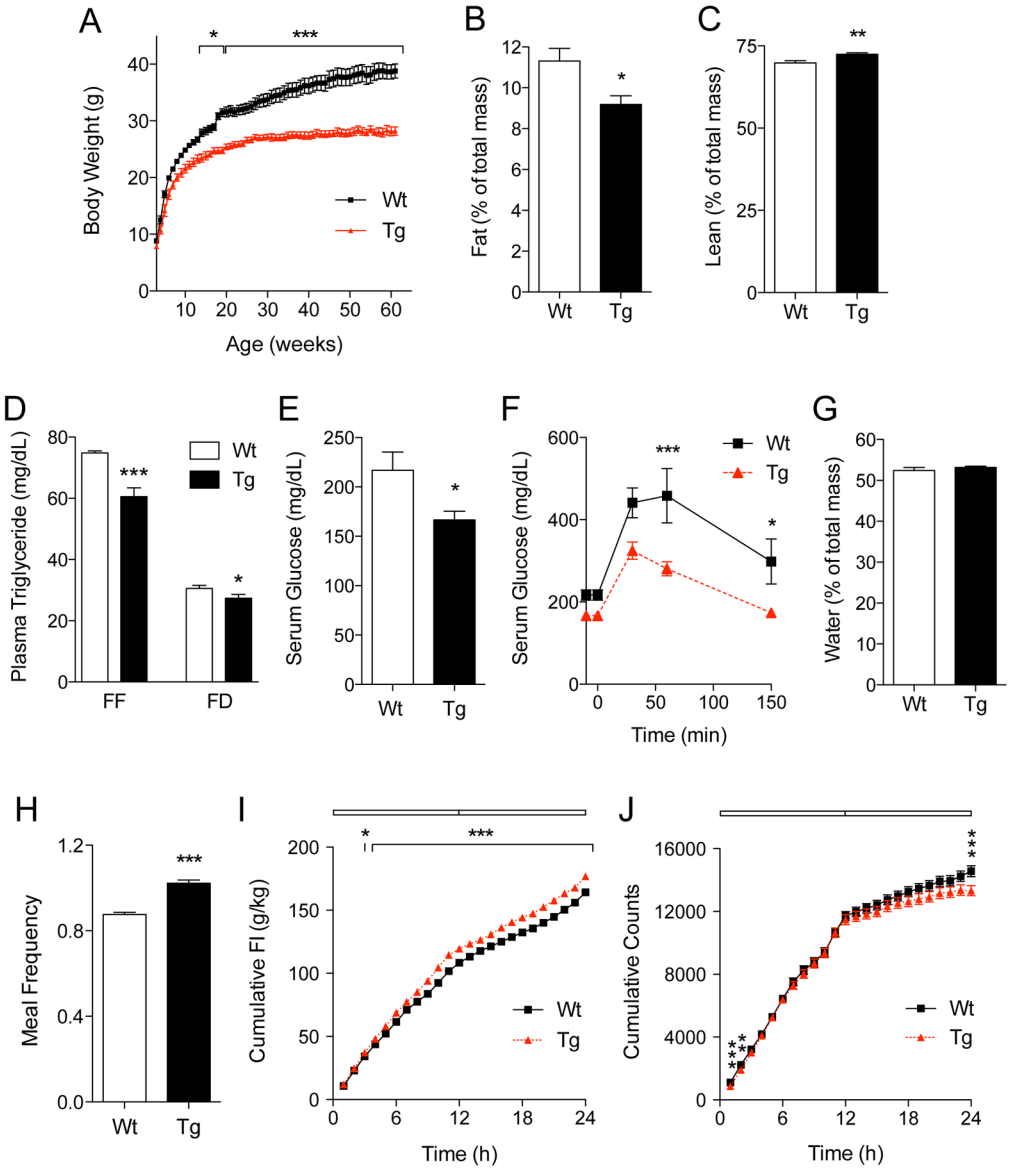

Figure 3. MGL-Tg mice are lean, hyperphagic and hypoactive

(A) Body-weight trajectory in wild-type (squares) and MGL-Tg mice (triangles) kept on a standard diet. *p<0.05 and ***p<0.001 (n=10).

(B–C) Body adiposity (B) and lean mass (C) in 20 week-old wild-type (Wt, open bars) and MGL-Tg mice (closed bars), as assessed by magnetic resonance imaging. *p<0.05 and **p<0.01 (n=8).

(D) Plasma triglycerides levels (mg/dl) in free-feeding (FF) or 4-h food-deprived (FD) wild-type (open bars) and MGL-Tg mice (closed bars). *p<0.05 and ***p<0.001 (n=3).

(E) Serum glucose levels (mg/dl) in 4-h food-deprived wild-type (open bars) and MGL-Tg mice (closed bars). *p<0.05 (n=5).

(F) Time-course (min) of glucose uptake (mg/dl) in wild-type (squares) and MGL-Tg mice (triangles). *p<0.05 and ***p<0.001 (n=5).

(G) Water body content (% body mass) of 20 week-old wild-type (Wt, open bars) and MGL-Tg mice (closed bars), as assessed by MRI (n=8).

(H) Meal frequency (number of meals/h) in adult wild-type (Wt, open bars) and MGL-Tg mice (closed bars). ***$p<0.001$ (n=10).
(I) Time-course (h) of daily food intake in adult wild-type (squares) and MGL-Tg mice (triangles). *$p<0.05$ and ***$p<0.001$ (n=10).
(J) Time-course (h) of daily motor activity (cumulative counts) in adult wild-type (squares) and MGL-Tg mice (triangles). **$p<0.01$ and ***$p<0.001$ (n=10 each).

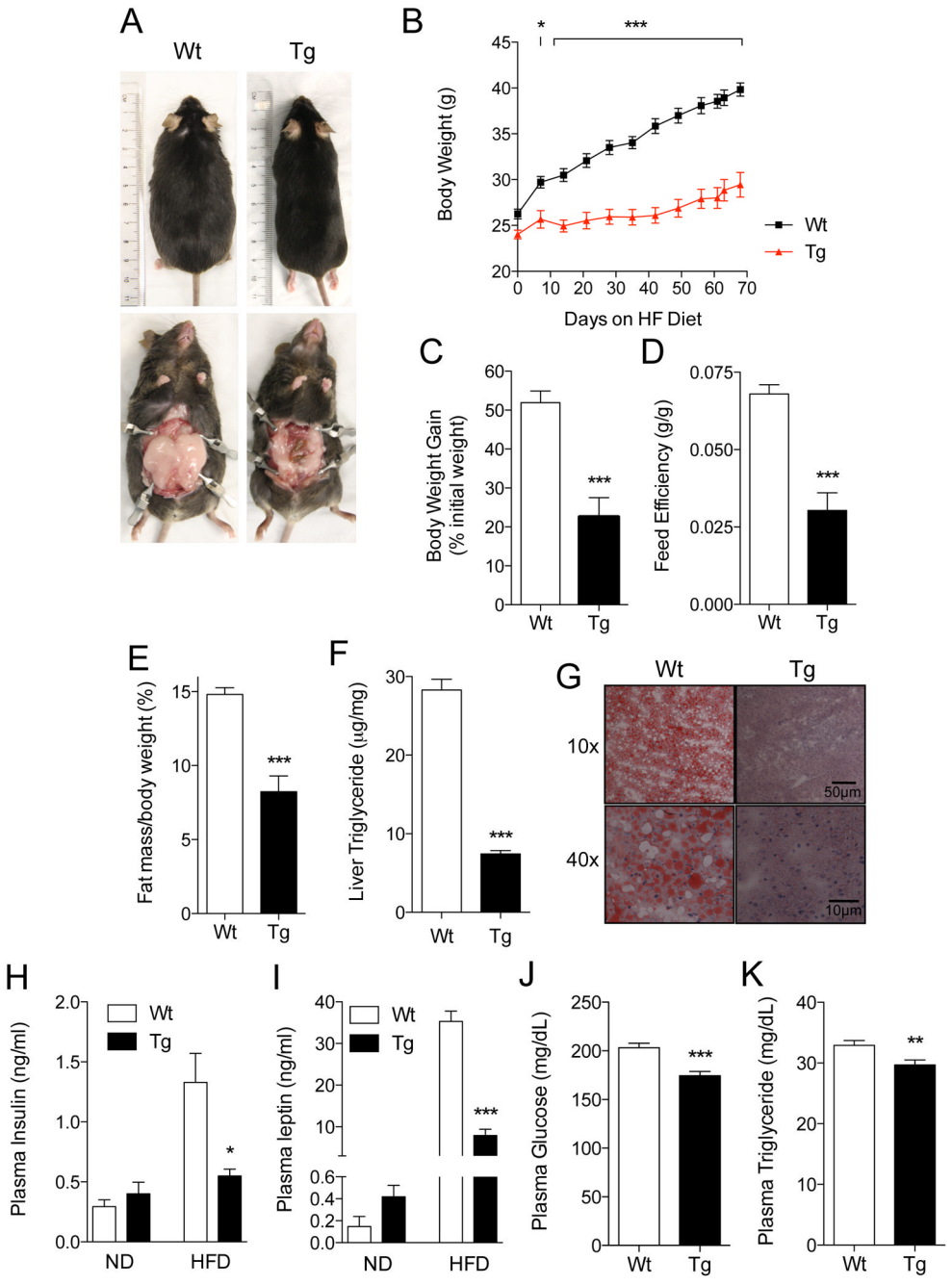

Figure 4. MGL-Tg mice are resistant to high-fat diet-induced obesity

(A) Representative images of wild-type (Wt) and MGL-Tg mice (Tg) after 10 weeks of high-fat diet.

(B) Body-weight trajectories (g) in wild-type mice (squares) and MGL-Tg mice (triangles) maintained on a high fat diet. *p<0.05 and ***p<0.001 (n=5–6).

(C–E) Body weight gain (% initial body weight) (C), feed efficiency (g body weight/g food intake) (D), and fat mass (% body weight) (E) in wild-type (open bars) and MGL-Tg mice (closed bars) kept on a high fat diet. ***p<0.001 (n=5–6).

(F) Triglyceride levels (μg/mg fresh tissue weight) in liver tissue from wild-type (open bars) and MGL-Tg mice (closed bars) kept on a high fat diet. ***p<0.001 (n=5–6).

(G) Neutral lipids staining (Oil Red O) in sections of liver tissue from wild-type (Wt) and MGL-Tg mice (Tg) kept on a high fat diet. Magnification: top, 10x; bottom, 40x.
(H–I) Plasma levels of insulin (H) and leptin (I) in wild-type (open bars) and MGL-Tg mice (closed bars) kept on normal (ND, n=3) or high-fat diet (HFD, n=5–6). *p<0.05 and ***p<0.001.
(J–K) Plasma levels of glucose (J) and triglycerides (K) in wild-type (open bars) and MGL-Tg mice (closed bars) kept on a high-fat diet. **p<0.01 and ***p<0.001 (n=5–6)

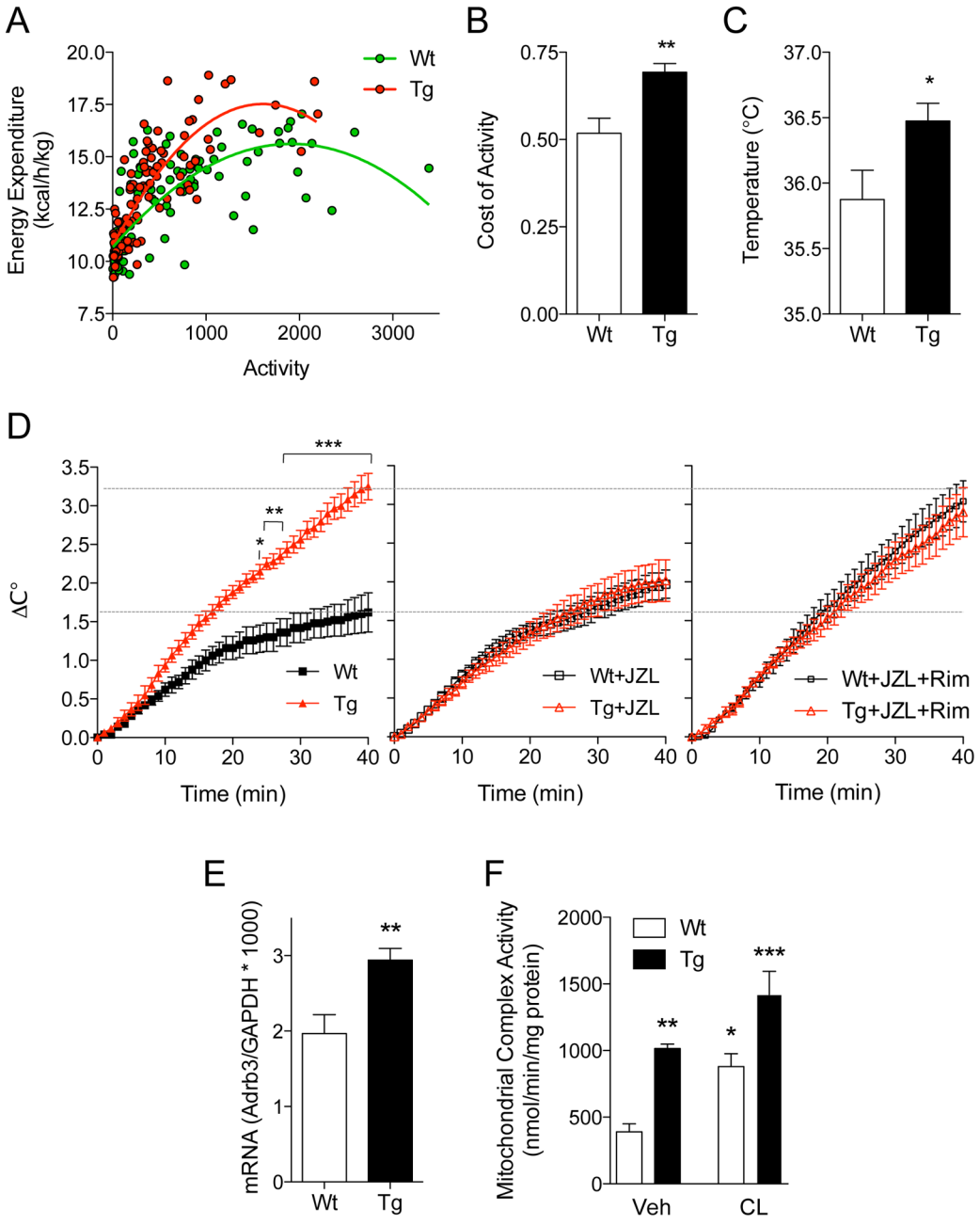

Figure 5. MGL-Tg mice have high energy cost of activity and are hypersensitive by β_3-adrenergic thermogenesis

(A) Regression analysis of energy expenditure (kcal/h/kg body weight) and motor activity (beam breaks) in wild-type (green circles) and MGL-Tg mice (red circles) kept on a normal diet.

(B) Energy cost of motor activity (slope of regression curve in A) in wild-type (Wt, open bars) and MGL-Tg mice (Tg, closed bars). $^{**}p<0.01$ (n=8).

(C) Average body temperature in wild-type (Wt, open bars) and MGL-Tg mice (tg, closed bars). $^{*}p<0.05$ (n=8).

(D) Time-course (min) of body temperature changes elicited by β_3-adrenergic agonist CL-316243 (0.1 mg/kg) in wild-type (squares) and MGL-Tg mice (triangles). CL-316243

was administered alone (left panel), together with MGL inhibitor JZL184 (16 mg/kg, 6 h before CL-316243) (center panel), or together with JZL184 plus CB_1 inverse agonist rimonabant (10 mg/kg) (right panel). *$p<0.05$, **$p<0.01$ and ***$p<0.001$ (n=5–7).
(E) Levels of mRNA encoding for β_3-adrenergic receptor in BAT from wild-type (Wt, open bars) and MGL-Tg mice (Tg, closed bars) fed with normal chow. **$p<0.01$ (n=3).
(F) Mitochondial complex activity (I + III) in BAT isolated from wild-type (Wt, open bars) and MGL-Tg mice (Tg, closed bars). *$p<0.05$, **$p<0.01$ and ***$p<0.001$ (n=3–4).

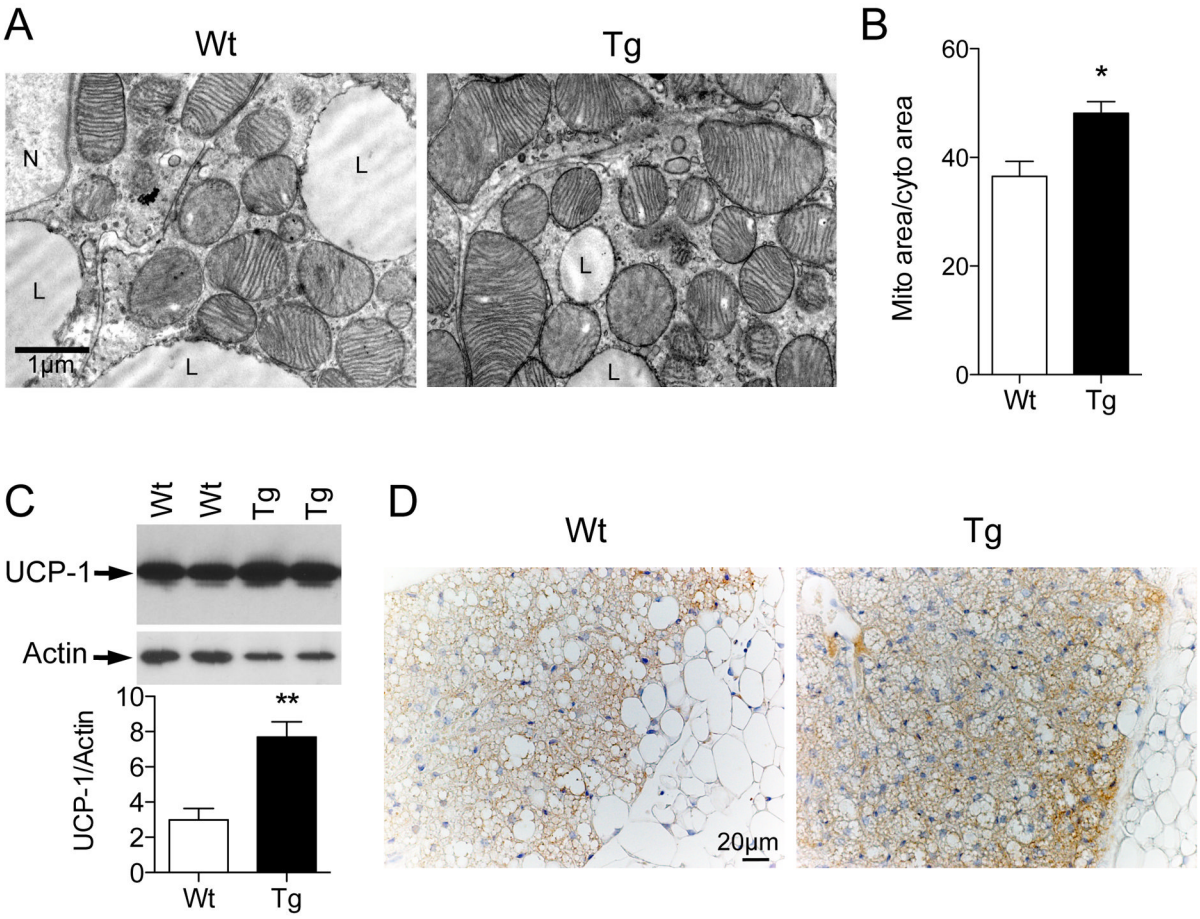

Figure 6. Increased mitochondria density in BAT of MGL-Tg mice

(A) Representative electron microscopy images of BAT from wild-type (Wt) and MGL-Tg mice (Tg). L, lipid vacuole; N, cell nucleus.

(B) Ratio of mitochondria area to cytosol area in BAT from wild-type (Wt, open bars) and MGL-Tg mice (Tg, closed bars) fed with normal chow. *p<0.05 (n=3–4).

(C–D). Levels of uncoupling protein-1 (UCP1) assessed by western blot analysis (C) or immunohistochemistry (D) in BAT from wild-type (Wt, open bars) and MGL-Tg mice (Tg, closed bars) fed with normal chow. Protein levels were quantified using the NIH Image J software and actin as a standard. **p<0.01 (n=4).

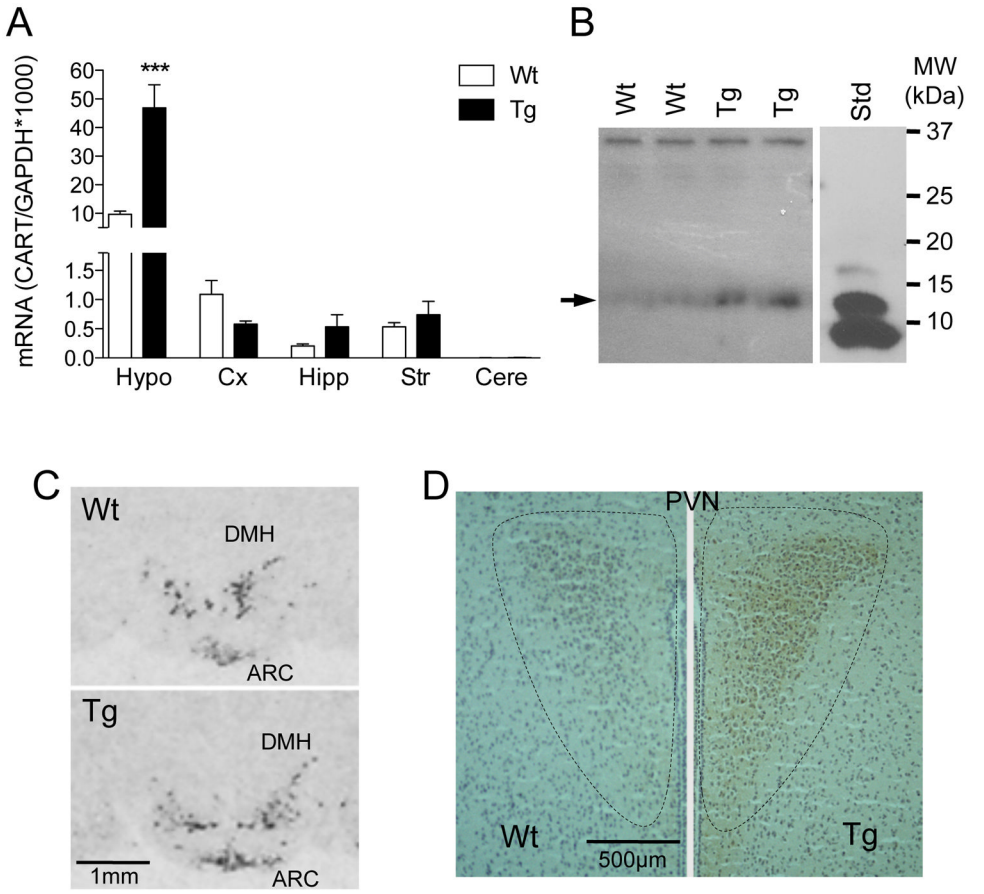

Figure 7. CART over-expression in the hypothalamus of MGL-Tg mice fed with normal chow

(A) CART mRNA levels in various brain regions of wild-type (Wt, open bars) and MGL-Tg mice (Tg, closed bars). ***p<0.001 (n=5–6).

(B) Western blot analyses of CART in the hypothalamus of wild-type (Wt) and MGL-Tg (Tg) mice. The arrow indicates the apparent molecular weight of synthetic CART (55–102), which is shown in the blot on the right (Std). Note that synthetic CART migrates as a monomer, dimer or trimer (6, 12 and 18 kDa, respectively). Results are from one experiment replicated 4 times with similar results.

(C) Localization of CART mRNA in the hypothalamus of wild-type (Wt) and MGL-Tg (Tg) mice. Abbreviations: ARC, arcuate nucleus; DMH, dorsomedial hypothalamus.

(D) Immunohistochemical localization of CART peptide in the hypothalamus of wild-type (Wt) and MGL-Tg (Tg) mice. Abbreviation: PVN, paraventricular nucleus.